Case study of absorption aerosol optical depth closure of black carbon over the East China Sea

M. Koike,[1] N. Moteki,[1] P. Khatri,[2] T. Takamura,[2] N. Takegawa,[3] Y. Kondo,[1] H. Hashioka,[1] H. Matsui,[1,4] A. Shimizu,[5] and N. Sugimoto[5]

Received 9 May 2013; revised 4 December 2013; accepted 5 December 2013.

[1] Absorption aerosol optical depth (AAOD) measurements made by sun-sky photometers are currently the only constraint available for estimates of the global radiative forcing of black carbon (BC), but their validation studies are limited. In this paper, we report the first attempt to compare AAODs derived from single-particle soot photometer (SP2) and ground-based sun-sky photometer (sky radiometer, SKYNET) measurements. During the Aerosol Radiative Forcing in East Asia (A-FORCE) experiments, BC size distribution and mixing state vertical profiles were measured using an SP2 on board a research aircraft near the Fukue Observatory (32.8°N, 128.7°E) over the East China Sea in spring 2009 and late winter 2013. The aerosol extinction coefficients (b_{ext}) and single scattering albedo (SSA) at 500 nm were calculated based on aerosol size distribution and detailed BC mixing state information. The calculated aerosol optical depth (AOD) agreed well with the sky radiometer measurements ($2 \pm 6\%$) when dust loadings were low (lidar-derived nonspherical particle contribution to AOD less than 20%). However, under these low-dust conditions, the AAODs obtained from sky radiometer measurements were only half of the in situ estimates. When dust loadings were high, the sky radiometer measurements showed systematically higher AAODs even when all coarse particles were assumed to be dust for in situ measurements. These results indicate that there are considerable uncertainties in AAOD measurements. Uncertainties in the BC refractive index, optical calculations from in situ data, and sky radiometer retrieval analyses are discussed.

Citation: Koike, M., N. Moteki, P. Khatri, T. Takamura, N. Takegawa, Y. Kondo, H. Hashioka, H. Matsui, A. Shimizu, and N. Sugimoto (2014), Case study of absorption aerosol optical depth closure of black carbon over the East China Sea, *J. Geophys. Res. Atmos.*, *119*, doi:10.1002/2013JD020163.

1. Introduction

[2] Absorption aerosol optical depth (AAOD) is a key parameter to evaluate aerosol radiative forcing and atmospheric heating. AAOD is a measure of the column aerosol light absorption and is expressed as (1 − SSA) AOD, where SSA and AOD are the column single scattering albedo and aerosol optical depth, respectively. Black carbon (BC) is considered the dominant light absorber and is emitted into the atmosphere by incomplete anthropogenic combustion and biomass burning [*Bond et al*., 2013]. Organic aerosols (OAs) and dust particles also absorb solar radiation, especially in the ultraviolet region [e.g., *Dinar et al*., 2008; *Sokolik and Toon*, 1999; *Aoki et al*., 2005]. Currently, the only way to measure AAOD routinely and globally is ground-based radiation measurements, such as sun-sky photometer measurements performed by Aerosol Robotic Network (AERONET) [*Dubovik et al*., 2002] and Sky Radiometer Network (SKYNET) [*Nakajima et al*., 2007]. In fact, these data are the only constraint available for estimates of the global radiative forcing of BC or carbonaceous (BC + OA) aerosols [*Bond et al*., 2013; *Chung et al*., 2012].

[3] With regard to sun-sky (or sun) photometer AOD measurements, validation studies have been made by conducting closure experiments with in situ aircraft aerosol extinction measurements [e.g., *Redemann et al*., 2003; *Shinozuka et al*., 2007; *Esteve et al*., 2012]. Generally, good agreement between the two measurements (approximately 10–50%) has been obtained. However, for AAOD or SSA measurements, only a very limited number of closure experiments have been conducted despite their great importance. During an aerosol intensive observation period of the Department of Energy's Atmospheric Radiation Measurement (ARM) in Oklahoma in May 2003, column SSAs derived from Cimel sun-sky photometer measurements (part of AERONET) were compared with in situ aircraft measurements [*Ricchiazzi et al*., 2006]. On board the aircraft, aerosol absorption and scattering coefficients were measured using a particle soot absorption photometer (PSAP) and TSI

[1]Department of Earth and Planetary Science, Graduate School of Science, University of Tokyo, Tokyo, Japan.
[2]Center for Environmental Remote Sensing, Chiba University, Chiba, Japan.
[3]Research Center for Advanced Science and Technology, University of Tokyo, Tokyo, Japan.
[4]Japan Agency for Marine-Earth Science and Technology, Tokyo, Japan.
[5]National Institute Environmental Studies, Tsukuba, Japan.

Corresponding author: M. Koike, Department of Earth and Planetary Science, Graduate School of Science, University of Tokyo, Hongo 7-3-1, Bunkyo-ku, Tokyo, 113-0033, Japan. (koike@eps.s.u-tokyo.ac.jp)

2169-897X/14/10.1002/2013JD020163

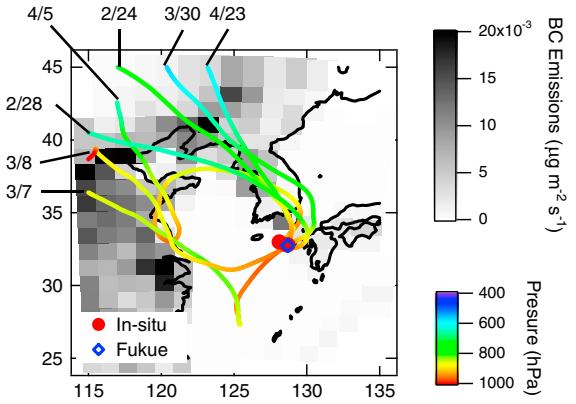

Figure 1. Five day kinematic back trajectories of air parcels sampled from aircraft (Table 1a) during seven spiral measurements (red dots). The 30 March, 5 April, and 23 April measurements were made in 2009, while the 24 and 28 February and 7 and 8 March measurements were made in 2013 (Table 1b). Each trajectory was calculated from 950 hPa, near the lowest measurement altitude. The location of Fukue Observatory is also shown (blue diamond). Trajectory colors indicate the atmospheric pressure along the trajectories. A BC emission inventory [*Streets et al.*, 2003] is shown using a gray scale.

integrating nephelometers, respectively, and column SSA was calculated using the following equation:

$$\mathrm{SSA}_{\mathrm{column}} = 1 - \frac{\mathrm{AAOD}}{\mathrm{AOD}} = \frac{\int \mathrm{SSA}(z).b_{\mathrm{ext}}(z)\mathrm{d}z}{\int b_{\mathrm{ext}}(z)\mathrm{d}z} \quad (1)$$

where b_{ext} is the aerosol extinction coefficient. As a result, the column SSAs agree to within approximately 0.05; the sun photometer measurements were lower by 0–5% and higher by 2–15% at 676 and 440 nm, respectively. In terms of SSA, the agreement is good, however; AAOD errors were in fact approximately 100% because the average SSA was approximately 0.95. A portion of the difference could be due to errors in in situ aerosol absorption measurements made with the PSAP, because these filter-based instruments are known to have uncertainties due to scattering of aerosols and complicated radiative transfer within filters [e.g., *Bond et al.*, 1999; *Arnott et al.*, 2005; *Moteki et al.*, 2010a; *Kondo et al.*, 2009]. Furthermore, PSAP is particularly unreliable for profiles because of its poor time resolution.

[4] Much better AAOD agreement with a mean difference of 19% at 500 nm was obtained between absorption photometer measurements (Magee Scientific, AE-31 aethalometer) on board aircraft and AERONET sun-sky photometer measurements at the Maldives [*Corrigan et al.*, 2008]. However, aethalometer and other filter-based measurements are generally known to have the uncertainties described above, and more validation studies are required. Although instruments for measuring aerosol absorption with greater accuracy have been developed in recent years, such as the photoacoustic spectrometer (PAS) [*Arnott et al.*, 2006] and photothermal interferometry (PTI) [*Sedlacek and Lee*, 2007], the accurate measurement of aerosol absorption on board aircraft remains a challenge.

[5] Another potential method for comparing sun-sky photometer AAOD measurements with in situ measurements is to calculate the optical properties of local aerosols from the aerosol size distribution, composition, and mixing state. Recently, detailed BC mass size distribution and mixing state information has been derived using the single-particle soot photometer (SP2) [e.g., *Moteki and Kondo*, 2007]. This is the only instrument that can provide the size and mixing state of individual BC particles, although some statistical information can also be obtained from the volatility tandem differential mobility analyzer (VTDMA) [e.g., *Cheng et al.*, 2009]. There are uncertainties in calculating aerosol optical properties from aerosol size and mixing state information, but these estimates are still useful when the uncertainties in in situ aerosol absorption measurements are considered.

[6] One of the difficulties in estimating the BC contribution to AAOD at visible wavelengths is that uncertainties arise from dust. Previous studies in East Asia and other regions have reported that SSAs are typically lower (more absorbing) when the atmospheric dust particle loading was higher [e.g., *Kim et al.*, 2005]. Generally, when BC-rich air is transported from the Asian continent to the Pacific in winter and spring, dust particles, whose source regions are located upstream from the BC sources, are potentially mixed.

[7] During the Aerosol Radiative Forcing in East Asia (A-FORCE) experiments conducted in spring 2009 [*Oshima et al.*, 2012] and late winter 2013 (denoted as the 2009 and 2013W experiments, respectively), vertical profiles of BC size distributions and mixing states were measured by an SP2 [*Moteki et al.*, 2012] with other aerosol parameters on board a research aircraft near the Fukue Observatory (32.8°N, 128.7° E) in the East China Sea. Using this data set, we calculate optical properties of local aerosols using the core-shell Mie scattering method by taking aerosol water uptake effects into account. The calculated AOD and AAOD are compared with ground-based measurements made with a sun-sky photometer, called as sky radiometer (Prede Co., Ltd., Tokyo, Japan), at the Fukue Observatory (part of SKYNET), to evaluate the AOD and AAOD closure. To our knowledge, an AAOD or column SSA closure study using SP2 measurements has not previously been reported, although only SP2 measurements can provide detailed BC mixing state information.

2. Measurements and Aerosol Optical Property Calculations

2.1. Aircraft Aerosol Measurements

[8] During the A-FORCE-2009 and -2013W experiments, aerosol vertical profiles were measured 3 and 4 times, respectively, near the Fukue Observatory (Figure 1 and Tables 1a and 1b). The mass of refractory BC (rBC, denoted as BC in this paper) with a mass-equivalent diameter (D_{BC}) between 75 and 850 nm and the thickness of coatings on BC were measured for individual BC-containing particles using an SP2 on board the aircraft [*Moteki et al.*, 2012]. The dominant uncertainty in measured BC mass concentrations lies in the sensitivity calibration to ambient BC particles, and it was estimated to be around 15% [*Moteki and Kondo*, 2010; *Kondo et al.*, 2011]. We assumed the void-free material density of BC to be 2 g cm^{-3} to convert BC mass to diameter D_{BC}. The thickness of the coating on BC (BC mixing state) was estimated from the scattering signal using a concentric

Table 1a. List of In Situ Measurements for A-FORCE-2009

Date (JST)	Time (JST)	Latitude[a]	Longitude[a]	Distance (km)	Lowest Altitude (km)
30 March	14:17	32.78	128.66	3.7	0.36
5 April	14:30	32.78	128.65	4.3	0.33
23 April	15:46	33.01	128.05	65.7	0.52

[a]The spiral descent diameter was typical 10 km; the pivot position is presented here.

coated-sphere model and assuming a refractive index of 1.52 at 1064 nm SP2 laser wavelength [*Moteki and Kondo*, 2007]. Dry aerosol size distributions (total particle size including BC and other aerosol compounds) for diameters (D) between 190 and 850 nm were also measured by the SP2 using the scattering signal for all aerosol particles (both BC-containing and BC-free particles) by assuming that they are spherical. All optical calculations were performed using the total aerosol size distributions and detailed BC mixing state information as described in the next section.

[9] During A-FORCE-2009, total aerosol number concentrations (N_{CN}) with dry diameters between 10 and 1000 nm and Aitken-mode aerosol concentrations with dry diameters between 10 and 130 nm were simultaneously measured using two condensation particle counters (TSI model 3771 and 3772 CPCs) and a low-pressure impactor [*Takegawa and Sakurai*, 2011; *Takegawa et al*., 2013]. Because the SP2 did not measure the complete aerosol size distribution, the aerosol size distribution smaller than 190 nm was estimated assuming a lognormal size distribution (single mode) using both SP2 and CPC data as described in *Koike et al*. [2012]. The BC mixing states for these smaller particles and particles with $D = 190$ nm were assumed to be identical. Namely, for particles with $D = 190$ nm, particle number fractions within individual D_{BC}/D ranges and a fraction of BC-free particles were calculated. These fractions were used for all particles smaller than $D = 190$ nm. The average contribution from this size range to the aerosol extinction (b_{ext}) and BC absorption (b_{abs} by coated BC) at the 500 nm wavelength was $3 \pm 2\%$ and $14 \pm 5\%$, respectively.

[10] During A-FORCE-2013W, size distributions for aerosols with dry diameters greater than 69 nm were measured using ultrahigh-sensitivity aerosol spectrometer (UHSAS). UHSAS data were used for the size range between 69 and 190 nm, while a lognormal size distribution was assumed for particles smaller than 69 nm. Similar to the A-FORCE-2009 experiment, the BC mixing states in this size range and for particles with $D = 190$ nm were assumed to be identical.

[11] In this study, we defined fine-mode aerosols as those having dry diameters smaller than 850 nm. To calculate the fine-mode aerosol size distributions for ambient relative humidity (RH) conditions, κ-Kohler theory was used [*Petters and Kreidenweis*, 2007]. We assumed that the BC coating material and BC-free particles consisted of ammonium sulfate, i.e., $(NH_4)_2SO_4$, and water, as for our previous study [*Koike et al*., 2012]. We used κ values for BC and $(NH_4)_2SO_4$ of 0.001 and 0.61, respectively (Table 2).

[12] The aerosol size distributions for ambient RH conditions with wet diameters greater than 600 nm were measured by a CAS (cloud and aerosol spectrometer) instrument with the laser scattering signal detection method [*Koike et al*., 2012]. CAS data were used for the size range greater than SP2 measurements, and aerosols in this size range were denoted as coarse particles in this study. Under dry ambient conditions ($RH < 30\%$), the SP2 and CAS measurements agree to within 20% for overlapping size ranges during the A-FORCE-2009 experiment. Because dust particles are important contributor for AAOD in East Asia, two different and simple assumptions for coarse particles were made. The first assumption was that all coarse particles were pure sea salt, i.e., NaCl. The aerosol water fraction was calculated using κ-Kohler theory and assuming a κ value of 1.12 for NaCl. The second assumption was that all coarse particles were pure dust with a κ value of 0.001. We denoted these two calculations as those with the "NaCl" and "dust" assumptions. In the dust assumption, both BC and dust were assumed to absorb light, while in the NaCl assumption, BC was the only absorber.

2.2. Calculations of Aerosol Optical Properties

[13] Aerosol optical properties were not measured on board the aircraft. Local aerosol optical properties at the 500 nm wavelength were calculated using the Mie theory algorithm developed by *Bohren and Huffman* [1998] assuming that all particles were spherical. For BC-containing particles, a BC concentric coated-sphere model was adopted (as for SP2 measurements), and the core-shell treatment code (BHCOAT) was used for optical calculations. The core-shell assumption was appropriate for the first approximation because during the A-FORCE-2013W experiment, filter sampling on board the aircraft followed by electron tomography [*Adachi et al*., 2010] indicated that most BC particles were coated (surrounded) with other aerosol compounds instead of being attached to BC-free particles or lacking a coating (K. Adachi, personal communication, 2013). The refractive index of the coating material (ammonium sulfate and water) was calculated using the volume average mixing rule. For BC-free particles, the well-mixed particles code (BHMIE) was applied. The core-shell and well-mixed particle treatments were used throughout this study

Table 1b. List of In Situ Measurements for A-FORCE-2013W

Date (JST)	Time (JST)	Latitude[a]	Longitude[a]	Distance (km)	Lowest Altitude (km)
24 February	11:31	32.76	128.69	1.2	0.19
28 February	15:01	32.76	128.69	1.2	0.18
7 March	14:29	32.76	128.69	1.2	0.33
8 March	13:17	32.77	128.68	2.0	0.21

[a]The spiral descent diameter was typical 10 km; the pivot position is presented here.

Table 2. Refractive Indices and Hygroscopicity Assumed for Optical Calculations

Compounds	Refractive Index at 500 nm	References for the Refractive Index	Hygroscopicity, κ [*Petters and Kreidenweis*, 2007; *Zaveri et al*., 2010]
BC base calculation	1.95 + 0.79i	*Bond and Bergstrom* [2006]	0.001
BC middle-level absorption	1.85 + 0.71i	*Bond and Bergstrom* [2006]	0.001
BC low-level absorption (OPAC)	1.74 + 0.44i	*Hess et al*. [1998]	0.001
BC high-level absorption	2.26 + 1.26i	*Moteki et al*. [2010a]	0.001
$(NH_4)_2SO_4$	1.53 + 0i	*Toon et al*. [1976]	0.61
NaCl	1.55 + 0i	*Toon et al*. [1976]	1.12
H_2O	1.335 + 0i	*Hale and Querry* [1973]	—
Organic compounds (other than HULIS)	1.45 + 0i	*Kanakidou et al*. [2005]	0.12
Organic compounds (HULIS)	1.59 + 0.039i	*Dinar et al*. [2008] and *Kirchstetter et al*. [2004]	0.12
Dust	1.51 + 0.0041i	*Aoki et al*. [2005]	0.001

except for sensitivity calculations (Maxwell-Garnett mixing treatment), which are presented in section 4. For the BC refractive index, the recommendation of *Bond and Bergstrom* [2006], i.e., $1.95 + 0.79i$, was used. Sensitivity calculations were also made using other values (section 4). The refractive indexes for other species are provided in Table 2.

[14] Local aerosol optical properties, namely b_{ext}, b_{abs}, SSA, and the asymmetry factor g, were calculated for the entire aerosol size distribution (fine and coarse particles). AOD and AAOD were calculated by vertically integrating b_{ext} and b_{abs}, respectively. Column SSA was calculated using equation 1. Because aircraft measurements were made at altitudes above 0.2–0.5 km (Tables 1a and 1b), the contribution from altitudes below the aircraft measurements were estimated by extrapolating the optical quantities at the lowest altitudes (five data averages, constant values) to the ground. This assumption (constant value) is reasonable because BC mass concentrations measured at the ground surface at the Fukue Observatory using a filter-based absorption photometer, the continuous soot monitoring system (COSMOS) [*Kanaya et al*., 2013], agree with the airborne SP2 data at the lowest altitudes within 24 ± 46% during the two A-FORCE experiments. The contributions to AOD and AAOD from the altitudes below the aircraft measurements were 14 ± 10% and 13 ± 8%, respectively ("dust" case). Uncertainties in the AAOD calculations are discussed in section 4.

2.3. Ground-Based Sky Radiometer Measurements

[15] The sky radiometer is a scanning sun-sky photometer, and the measurements at the Fukue Observatory have been made as part of a ground-based measurement network over Asia called SKYNET [*Nakajima et al*., 2007]. Direct irradiance and sky radiances at predefined scattering angles are measured with the sky radiometers, which are analyzed to derive aerosol column optical properties, such as the AOD, AAOD, SSA, and asymmetry factor g, using an algorithm developed for sky radiometer data retrievals, i.e., SKYRAD.pack version 4.2 [*Nakajima et al*., 1996; *Hashimoto et al*., 2012]. Note that SSA is assumed vertically uniform in this retrieval analysis, although in situ measurements indicate that SSA typically varies ± 0.02. The AAOD was estimated from the column SSA using equation 1.

[16] It has been reported that SKYNET AODs generally agree with the AERONET values, while SSAs are typically 3 to 8% higher (less absorbing) than the AERONET values at the Beijing site [*Che et al*., 2008]. The SSA positive bias compared with the AERONET measurements has also been observed at other sites and has been attributed to errors in the surface albedo, sky radiometer solid view angle, and/or cirrus contamination [*Hashimoto et al*., 2012]. An error in the surface albedo of −50% (0.1) can result in an SSA error of +3.7% at 500 nm.

[17] *Hashimoto et al*. [2012] proposed three data selection criteria for sky radiometer SSA measurements to remove low-quality or cloud-contaminated data. These criteria were adopted in this study except for the AOD (500 nm) criterion; *Hashimoto et al*. [2012] discarded data with AODs lower than 0.4 following the AERONET Level 2.0 quality control algorithm [*Dubovik et al*., 2000]. These data were cautiously used in this study, because only four of the seven cases could be used otherwise. It should be pointed that AODs lower than 0.4 are found for a large fraction of data at this site, indicating that these data were typical.

[18] During both A-FORCE experiments, aerosol optical properties were derived every 10 min using the sky radiometer at the Fukue Observatory. Because the aircraft vertical sounding over the Fukue Observatory typically required 30 min and fluctuations in individual sky radiometer data existed, 2 h averages were used for the sky radiometer measurements. The surface albedo used in the retrieval analyses was 0.048–0.057, which was estimated using Moderate Resolution Imaging Spectroradiometer (MODIS) data (3×3 km^2 average) obtained at the nearest date.

2.4. Ground-Based Lidar Measurements

[19] The lidar measurements at the Fukue Observatory were part of the lidar network over Asia, which is maintained by the National Institute for Environmental Studies (NIES) in Japan [*Shimizu et al*., 2004; *Katagiri et al*., 2010]. The extinction coefficient, b_{ext}, has been retrieved from the backscattering coefficient at 532 nm. The depolarization ratio has also been obtained so that contributions from spherical (mostly from fine particles and sea salt under humid conditions) and nonspherical (mostly dust) particles can be estimated. The contribution of nonspherical particles to the total AOD (spherical + nonspherical) was between 8 and 90% for the cases examined in this study.

[20] Lidar data recorded every 15 min over a 30 min period (i.e., 3 data points) were averaged and used in this study. The Fukue Observatory is located 80 m above sea level, and b_{ext} data are obtained in every 30 m layer at altitudes above 200 m. To calculate the AOD, b_{ext} between 200 and 350 m (average of 5 points) was extrapolated to the ground. The contributions from

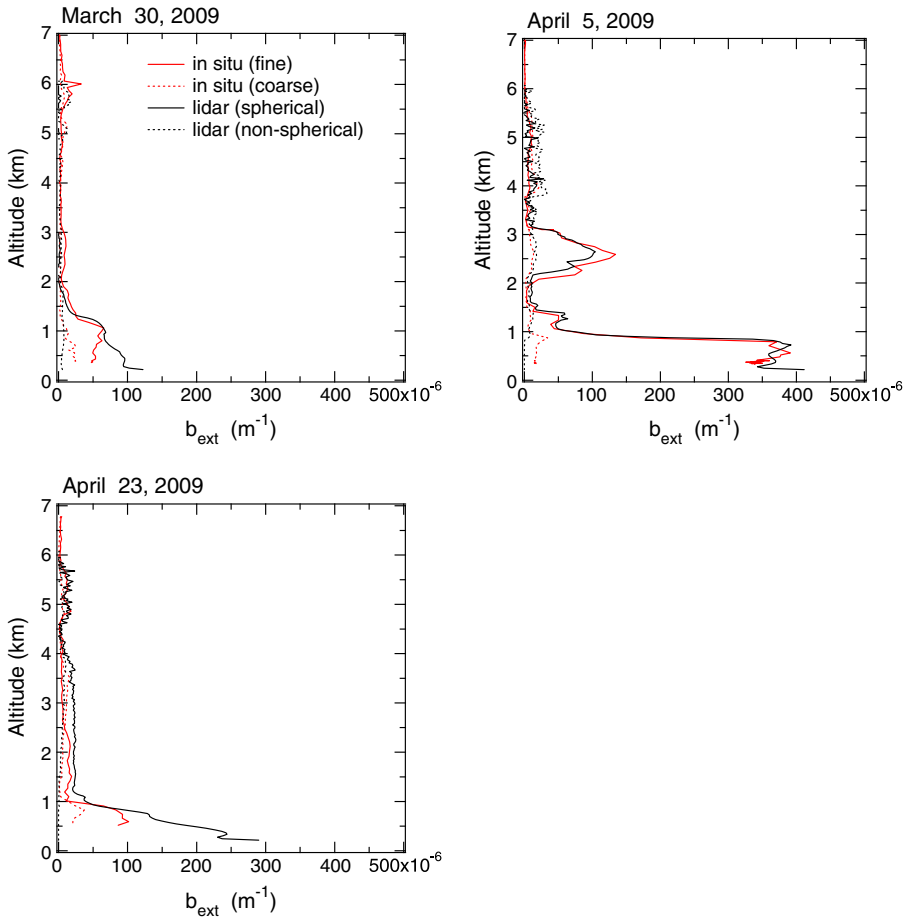

Figure 2. Comparison of aerosol extinction (b_{ext}) derived from aircraft and lidar measurements at 532 nm for the A-FORCE-2009 experiment. Aircraft values were calculated from in situ measurements of the aerosol size distribution and BC mixing state assuming all coarse particles were dust. In general, the fine and coarse particle b_{ext} values agree with spherical and nonspherical particle b_{ext} values, respectively, suggesting that most coarse particles were dust.

total (spherical + nonspherical) particles in this altitude range to the AOD were 13 ± 4%.

3. Intercomparison Between Aircraft and Ground-Based Observations

3.1. Vertical Profile

[21] Figure 1 shows 5 day kinematic backward trajectories of air parcels sampled from the aircraft at pressure altitudes near 950 hPa during the vertical sounding. Trajectories for both the 2009 and 2013W cases are shown. The trajectories were calculated using the National Centers for Environmental Prediction (NCEP) final (FNL) operational global analysis data and an algorithm developed by *Tomikawa and Sato* [2005]. BC emissions [*Streets et al*., 2003] are also shown in Figure 1. Air parcels within the boundary layer were generally transported from over the Korean Peninsula and northeastern China where large cities with high BC emissions, such as Beijing, are located.

[22] Figures 2 (2009 data) and 3 (2013W data) compare aerosol extinction (b_{ext}) vertical profiles derived from in situ (fine and coarse particles) and lidar (spherical and nonspherical particles) measurements. In these figures, b_{ext} values at 532 nm are shown for in situ measurements as an exception. The b_{ext} values at 500 nm are exclusively shown for in situ measurements throughout the rest of this paper. Results for the dust assumption are shown in Figures 2 and 3; the results for the NaCl assumption exhibit only small changes (AOD changes are less than 1%). In general, a good agreement is found between fine (in situ) and spherical particles (lidar) and between coarse (in situ) and nonspherical particles (lidar). This result suggests that fine particles are primarily spherical (solution droplets which may contain BC), whereas a considerable fraction of the coarse particles are dust. A portion of the coarse particles observed at altitudes below 1 km on 30 March and 23 April (Figure 2) may be spherical because the contributions from coarse particles are systematically greater than from nonspherical particles, while contributions from fine particles are systematically lower than from spherical particles. In fact, the total extinction (fine + coarse and spherical + nonspherical) agrees better than the individual contributions (not shown). Moreover, a portion of fine particles at altitudes below 2 km on 7 March (Figure 3) may be nonspherical. Although the correspondences between fine and spherical particles and between coarse and nonspherical particles are not perfect, it is reasonable to assume as a first approximation that most coarse particles observed on these days are dust.

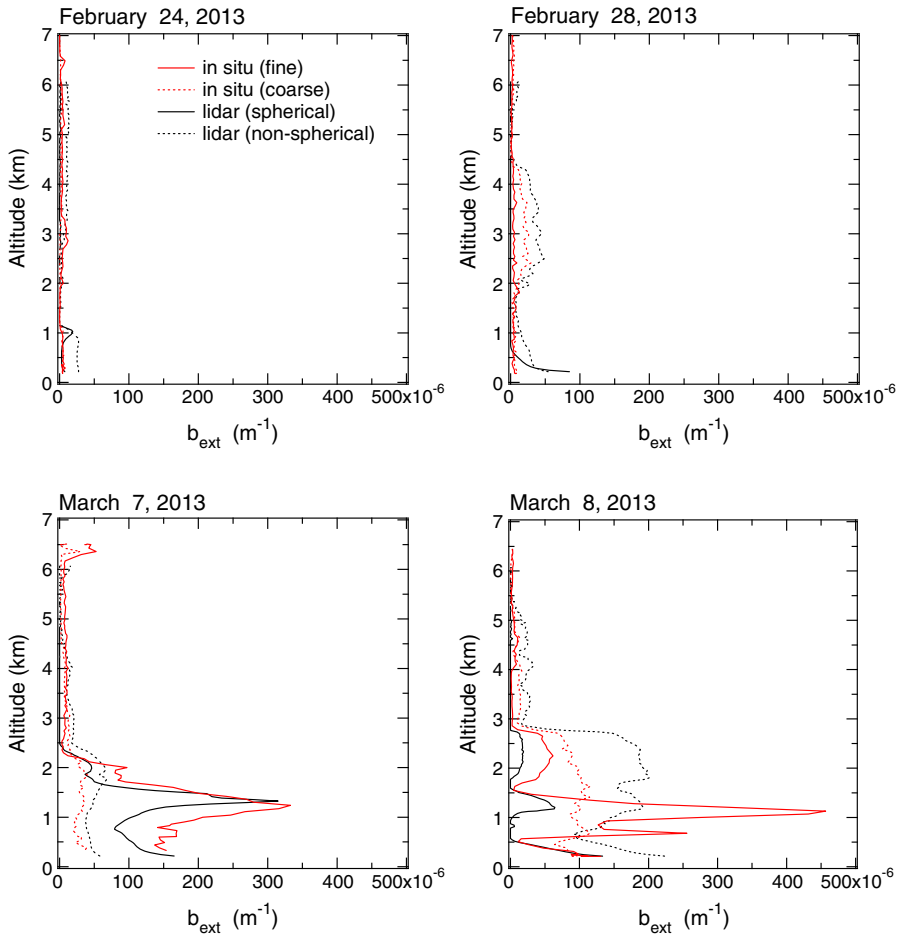

Figure 3. Same as Figure 2 except for the A-FORCE-2013W experiment.

[23] Relatively large discrepancies are found for the 8 March case (Figure 3). When the lidar data obtained at 15 min intervals were examined, a large temporal variation was found, suggesting large spatial variability in aerosols (not shown). Nevertheless, agreements in the seven cases suggest that both lidar measurements and aerosol extinction calculations from in situ aerosol measurements are reasonably accurate. The agreements also ensure that these aircraft and ground-based measurements were made in air with similar aerosol characteristics, confirming that the comparison between aircraft and ground-based sky radiometer measurements is reasonable.

3.2. Column Amount

[24] Figure 4 shows AOD comparisons between sky radiometer measurements and in situ or lidar measurements (at 500 nm except for lidar measurements, which are provided at 532 nm). These results are also tabulated in Tables 3a and 3b. Error bars for the in situ measurements are uncertainties (random errors) in the contribution from the altitudes below the aircraft measurements (100% error is assumed). When other more or less systematic uncertainty sources are considered, the uncertainties become greater (especially for the AAOD as described in section 4). For sky radiometer and lidar measurements, one standard deviation is shown as random errors.

[25] We introduce two measures to classify the data. The first measure is the AOD. The AODs are used to divide the data into two groups, one with relatively high aerosol loading (AOD $>$ 0.5, 5 April 2009 and 7 and 8 March 2013) and the other with relatively low aerosol loading (AOD $<$ 0.2). According to the data selection criteria of both AERONET [*Dubovik et al.*, 2000] and SKYNET [*Hashimoto et al.*, 2012], SSA retrievals are reliable only for AODs greater than 0.4. However, we used data with AODs $<$ 0.4 with caution as described above. The second measure for data classification is the dust fraction, which was evaluated as the lidar-derived nonspherical particle contribution to the total AOD. Specifically, when this fraction was less than 20% and greater than 40%, data were classified as "low-dust" and "high-dust" cases, respectively. As a result, all 2009 and 2013W data are classified into the low-dust and high-dust cases, respectively. The results of these two classifications are listed in Tables 3a and 3b. Considering the AERONET and SKYNET criteria for reliable SSA retrieval, i.e., AOD $>$ 0.4 ("high-AOD"), 5 April is the only low-dust case. Therefore, this case is examined in detail in the next section. For the high-dust condition, 7 and 8 March satisfy the high-AOD criterion. These data are also examined later.

[26] The AODs calculated from in situ measurements (Figure 4, red circles) agree with the sky radiometer measurements to within 12 $\pm$ 18% (RMS difference of 19%) for the high-AOD cases. When low-dust cases are selected

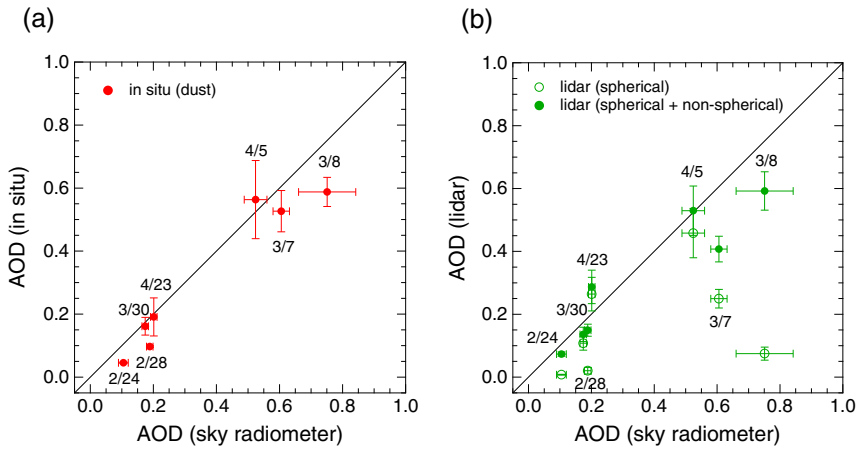

Figure 4. Comparison of AOD between (a) aircraft (in situ) and sky radiometer measurements and (b) lidar and sky radiometer measurements. The AODs at the 500 nm wavelength are shown for in situ and sky radiometer measurements, while values at 532 nm are shown for the lidar measurements. In situ values were calculated assuming all coarse particles were dust, although only a small change resulted when the NaCl (+ water) assumption was adopted (less than 1%). In situ data uncertainties (error bars) were estimated from the contribution from altitudes below the aircraft soundings. The lidar and sky radiometer uncertainties were the standard deviations within each averaging period. The agreement between in situ and sky radiometer measurements is generally good for the low-dust cases (30 March, 5 April, and 23 April).

(including "low-AOD" cases), the agreement is within $2 \pm 8\%$ (RMS difference of 8%). These results suggest high accuracies of both sky radiometer measurements and aerosol optical calculations from the in situ measurements, especially in low-dust conditions (Tables 3a and 3b). The average difference increases ($39 \pm 52\%$) when low-AOD and high-dust data (such as 24 and 28 February) are included. The AODs estimated from lidar measurements (spherical + nonspherical) agree with the in situ measurements to within $-9 \pm 12\%$ (RMS difference of 13%) and $17 \pm 36\%$ for high-AOD data and all data, respectively.

[27] Figures 5a and 5b show a comparison of the AAODs. They show a clear contrast between the low-dust (Figure 5a) and high-dust cases (Figure 5b). In the low-dust cases (30 March and 5 and 23 April), the AAODs are approximately 3 to 5 times greater than the sky radiometer measurements when the dust assumption is utilized to calculate the AAODs from in situ data (red circles). Even when the NaCl assumption (BC is the only absorber) is utilized for these cases, the AAODs remain 2 to 3 times greater (blue circles). On the other hand, the in situ AAODs are systematically lower even when the dust assumption is utilized for the high-dust cases (24 and 28 February and 7 and 8 March). This tendency is confirmed by Figure 6, which presents a scatter plot between AAOD (in situ)/AAOD (sky radiometer) ratios and AOD (lidar, nonspherical)/AOD (lidar, spherical + nonspherical) ratios. The cases in which the in situ AAODs are greater than the sky radiometer measurements correspond to the low-dust conditions (nonspherical AOD contributions are 10–20%), while the lower in situ AAODs correspond to high-dust loading conditions (80–90% except for the 7 March case). The SSAs are consistent with these AAODs (Figures 5c and 5d). In the following two sections, the low- and high-dust cases are examined in more detail.

[28] Before providing a detailed discussion on AAODs, we show in Figure 7 that the asymmetry factors (g) from sky radiometer measurements and estimates from in situ aerosol measurements agree well, i.e., within 3% on average. This result suggests that the aerosol size distribution estimated from sky radiometer measurements is reasonably accurate, in terms of the asymmetry factor for these particular cases.

3.3. Low-Dust Case: 5 April

[29] The 5 April case is further examined, because it is the only case in which both the high-AOD (AOD > 0.4) and low-dust (contribution from dust light absorption is expected to be small) requirements were satisfied. The AAOD retrieved from the sky radiometer measurements is a factor of 2 smaller (50% smaller) than in situ measurement estimates even when the NaCl assumption is adopted. In accordance with this result, the SSA (Figure 5c, blue circle) is systematically higher for sky radiometer measurements by approximately 0.019 (2.0%). Although the AODs are lower than 0.4, both the 30 March and 23 April cases exhibit similar results; all three low-dust cases indicate that sky radiometer-derived AAODs are systematically lower than the in situ estimates by 50–65% (NaCl assumption). Possible uncertainties for the estimates from in situ data are described in section 4.

[30] When the column average BC mass absorption cross section (MAC) was calculated using sky radiometer-derived AAOD and column BC mass (M_{BC}) obtained from in situ measurements (MAC = AAOD/M_{BC}), 3.11 ± 0.19 m^2 g^{-1} was obtained for 5 April. In this calculation, the column BC mass was estimated by vertically integrating the BC mass concentration obtained from in situ measurements and adding the mass concentrations at altitudes below the aircraft measurements (20% of M_{BC}), which is analogous to the process used for AAOD calculations (see section 2.2). MAC values measured for freshly generated BC were reported to be 7.5 ± 1.2 m^2 g^{-1} at 550 nm wavelength, and they tend to increase when BC particles are coated by other aerosol compounds [*Bond and Bergstrom*, 2006; *Bond et al.*, 2013]. The MAC estimated from the sky radiometer is systematically lower, suggesting an underestimation in

Table 3a. Intercomparison Summary for A-FORCE-2009 (Low-Dust Cases)[a]

		Assumed Coarse Particles for In Situ Measurements	30 March (Low-AOD, Low-Dust)	5 April (High-AOD, Low-Dust)	23 April (Low-AOD, Low-Dust)	Average ± SD	RMS diff.
AOD	in situ	dust	0.162 ± 0.028	0.563 ± 0.124	0.191 ± 0.060	0.305 ± 0.183	
		NaCl	0.163 ± 0.029	0.566 ± 0.125	0.192 ± 0.061	0.307 ± 0.184	
	lidar (spherical + non-s)	—	0.136 ± 0.023	0.530 ± 0.078	0.287 ± 0.053	0.318 ± 0.162	
	sky radiometer	—	0.174 ± 0.010	0.524 ± 0.036	0.201 ± 0.010	0.300 ± 0.159	
	diff (lidar − in situ) (%)	dust	−15.8	−5.97	50.4	9.52 ± 29.2	19.9
		NaCl	−16.6	−6.41	49.5	8.84 ± 29.0	19.8
	diff (skyrad − in situ) (%)	dust	7.70	−6.92	5.26	2.01 ± 6.40	7.98
		NaCl	6.77	−7.37	4.66	1.35 ± 6.23	8.28
AAOD	in situ	dust	0.0128 ± 0.0023	0.0291 ± 0.0052	0.0141 ± 0.0038	0.0187 ± 0.0074	
		NaCl	0.0074 ± 0.0011	0.0222 ± 0.0044	0.0074 ± 0.0022	0.0123 ± 0.0070	
	sky radiometer	—	0.0032 ± 0.0014	0.0111 ± 0.0071	0.0025 ± 0.0017	0.0056 ± 0.0039	
	diff (skyrad − in situ) (%)	dust	−75.0	−62.0	−81.9	−73.0 ± 8.27	72.6
		NaCl	−56.4	−50.2	−65.9	−57.5 ± 6.46	60.2
SSA	in situ	dust	0.921 ± 0.020	0.948 ± 0.015	0.926 ± 0.031	0.932 ± 0.012	
		NaCl	0.955 ± 0.010	0.961 ± 0.012	0.961 ± 0.017	0.959 ± 0.003	
	sky radiometer	—	0.982 ± 0.008	0.980 ± 0.013	0.987 ± 0.009	0.983 ± 0.003	
	diff (skyrad − in situ) (%)	dust	6.63	3.30	6.57	5.50 ± 1.56	5.50
		NaCl	2.82	1.96	2.70	2.49 ± 0.38	2.52
g	in situ	dust	0.666	0.714	0.675	0.685 ± 0.021	
		NaCl	0.664	0.714	0.666	0.681 ± 0.023	
	sky radiometer	—	0.656 ± 0.012	0.708 ± 0.012	0.669 ± 0.006	0.678 ± 0.022	
	diff (skyrad − in situ) (%)	dust	−1.42	−0.88	−1.00	−1.10 ± 0.23	1.11
		NaCl	−1.23	−0.76	0.40	−0.53 ± 0.68	0.86

[a]Uncertainties in in situ data were estimated from the contribution from altitudes below the aircraft soundings. Uncertainties in lidar and sky radiometer measurements are the standard deviation of the data within each averaging period. "non-s" stands for nonspherical; "diff" stands for difference; and "skyrad" stands for sky radiometer.

Table 3b. Intercomparison Summary for A-FORCE-2013W (High-Dust Cases)[a]

		Assumed Coarse Particles for In Situ Measurements	24 February (Low-AOD, High-Dust)	28 February (Low-AOD, High-Dust)	7 March (High-AOD, High-Dust)	8 March (High-AOD, High-Dust)	Average ± SD	RMS diff.
AOD	in situ	dust	0.046 ± 0.003	0.097 ± 0.003	0.527 ± 0.066	0.588 ± 0.046	0.314 ± 0.245	
		NaCl	0.046 ± 0.003	0.097 ± 0.003	0.530 ± 0.067	0.591 ± 0.046	0.316 ± 0.246	
	lidar (spherical + non-s)	—	0.074 ± 0.007	0.149 ± 0.019	0.407 ± 0.041	0.592 ± 0.061	0.306 ± 0.207	
	sky radiometer	—	0.105 ± 0.016	0.189 ± 0.010	0.606 ± 0.026	0.751 ± 0.091	0.413 ± 0.272	
	diff (lidar − in situ) (%)	dust	60.9	53.6	−22.6	0.79	23.2 ± 35.2	21.2
		NaCl	60.0	53.3	−23.1	0.29	22.6 ± 35.0	21.5
	diff (skyrad − in situ) (%)	dust	130	94.2	15.0	27.8	66.7 ± 47.2	33.7
		NaCl	128	93.8	14.3	27.2	65.9 ± 47.0	32.9
AAOD	in situ	dust	0.0055 ± 0.0004	0.0123 ± 0.0005	0.0391 ± 0.0042	0.0625 ± 0.0044	0.0299 ± 0.0226	
		NaCl	0.0039 ± 0.0002	0.0040 ± 0.0003	0.0265 ± 0.0028	0.0268 ± 0.0023	0.0153 ± 0.0114	
	sky radiometer	—	0.0039 ± 0.0022	0.0175 ± 0.0034	0.0599 ± 0.0080	0.1033 ± 0.0208	0.0462 ± 0.0389	
	diff (skyrad − in situ) (%)	dust	−28.6	41.5	53.2	65.5	32.9 ± 36.5	77.3
		NaCl	1.35	336	126	286	187 ± 132	277
SSA	in situ	dust	0.879 ± 0.011	0.873 ± 0.006	0.926 ± 0.012	0.894 ± 0.011	0.893 ± 0.020	
		NaCl	0.916 ± 0.007	0.959 ± 0.003	0.950 ± 0.008	0.955 ± 0.005	0.945 ± 0.017	
	sky radiometer	—	0.963 ± 0.019	0.907 ± 0.020	0.901 ± 0.012	0.863 ± 0.019	0.909 ± 0.036	
	diff (skyrad − in situ) (%)	dust	9.49	3.90	−2.66	−3.41	1.83 ± 5.26	5.50
		NaCl	5.16	−5.42	−5.15	−9.57	−3.75 ± 5.43	6.62
g	in situ	dust	0.612	0.691	0.717	0.712	0.683 ± 0.042	
		NaCl	0.609	0.671	0.714	0.699	0.673 ± 0.040	
	sky radiometer	—	0.653 ± 0.008	0.688 ± 0.008	0.712 ± 0.010	0.702 ± 0.012	0.689 ± 0.022	
	diff (skyrad − in situ) (%)	dust	6.71	−0.35	−0.71	−1.43	1.05 ± 3.29	3.12
		NaCl	7.23	2.54	−0.32	0.37	2.45 ± 2.95	3.51

[a]Uncertainties in in situ data were estimated from the contribution from altitudes below the aircraft soundings. Uncertainties in lidar and sky radiometer measurements are the standard deviation of the data within each averaging period. "non-s" stands for nonspherical; "diff" stands for difference; and "skyrad" stands for sky radiometer.

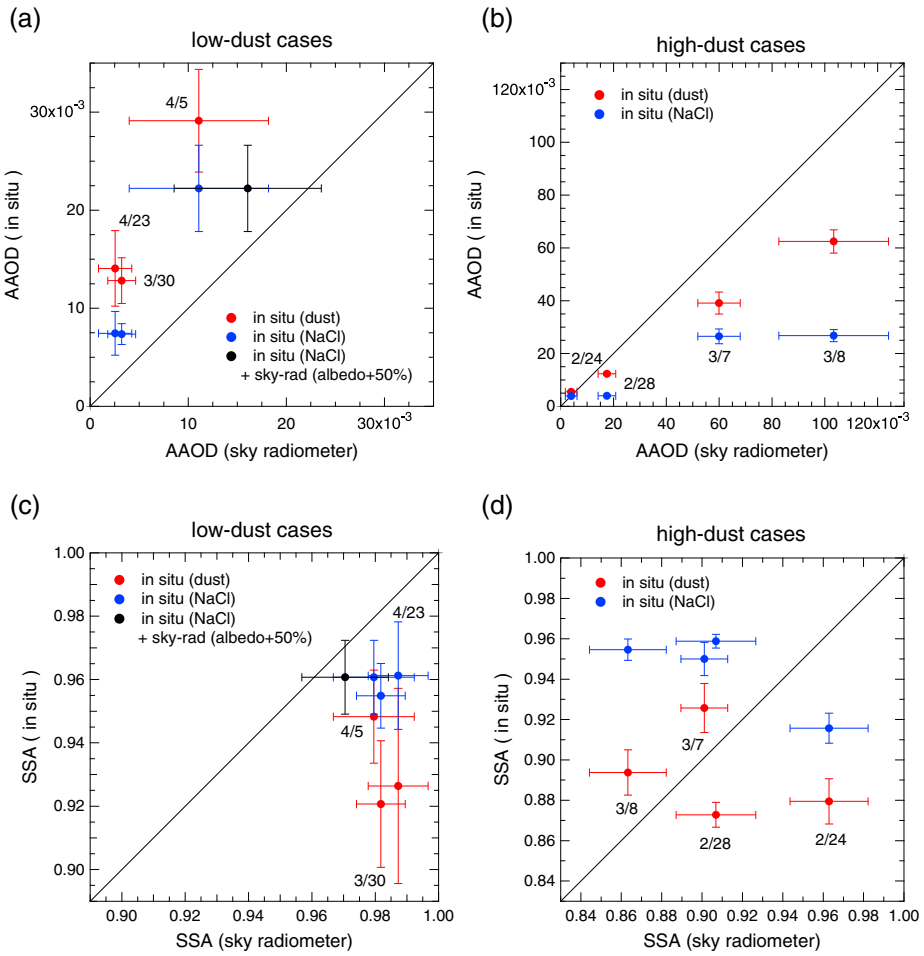

Figure 5. Comparison of AAOD and SSA between aircraft (in situ) and sky radiometer measurements. Red and blue circles denote results obtained assuming all coarse particles (in situ measurements) are dust and NaCl (+ water), respectively. Black circles denote values estimated from sky radiometer measurements assuming a 50% higher surface albedo indicating the uncertainty in the sky radiometer retrievals (values are shown only for 5 April case). Uncertainties (error bars) are the same as in Figure 4. When compared with the in situ measurement-derived AAODs, the sky radiometer-derived AAODs are systematically lower and higher in low-dust and high-dust cases, respectively. In accordance with this result, sky radiometer-derived SSAs are, in general, systematically higher and lower in low-dust and high-dust cases, respectively.

sky radiometer-derived AAOD. If dust particles contributed to light absorption, the MAC becomes even smaller. Although the MAC can also be calculated using in situ AAOD data, a good agreement (7.44 ± 0.73 m^2 g^{-1}) with the previous measurements indicates that the Mie optical calculations and the previous measurements agree well. Because only one case was available with both high-AOD and low-dust conditions and the M_{BC} estimate from in situ measurements contains uncertainties, we do not conclude that AAODs derived from the sky radiometer have a negative bias. However, systematically lower AAODs or higher SSAs have been reported from sky radiometer measurements compared with AERONET measurements [*Che et al.*, 2008; *Hashimoto et al.*, 2012], where even larger differences were found. Because the atmospheric heating rate is generally proportional to the AAODs, more accurate measurements are necessary to constrain model calculations.

[31] One possible reason for the negative bias in the sky radiometer AAOD measurements is the error in the surface albedo used for the retrieval analyses. By adopting the assumption made in *Hashimoto et al.* [2012], AAODs and SSAs were estimated using a 50% higher surface albedo (0.072 instead of 0.048; Figures 5a and 5c, black circles). The Fukue Observatory is located near the center of a peninsula (4.5×4.5 km^2) on the Fukue Island (18×18 km^2). Therefore, we speculated that the ground reflectance near the observatory could potentially affect the sky radiometer measurements. Figure 5a shows that the AAOD increases by 71%, resulting in a better agreement with in situ measurements for both AAOD and SSA. The increase in AAOD is required in the retrieval analysis to compensate the increase in the diffuse solar radiation resulted from the higher surface albedo assumption. This result indicates that an accurate surface albedo estimate is an important step to accurately determine AAODs and SSAs from ground-based radiation measurements.

3.4. High-Dust Case: 7 and 8 March

[32] The 7 and 8 March cases are classified as high AOD and high dust. The AAODs for the in situ dust assumption are systematically lower than the sky radiometer estimates. There

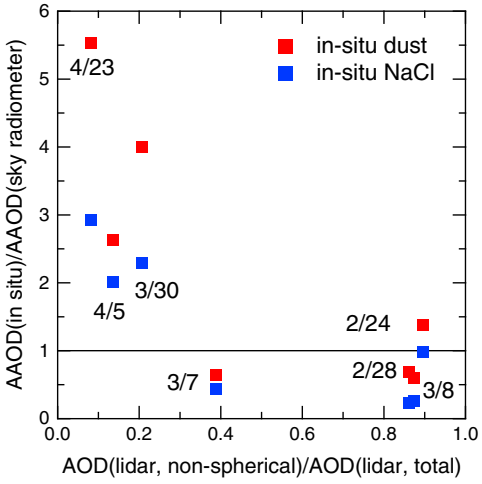

Figure 6. A scatter plot between AAOD (in situ)/AAOD (sky radiometer) ratios and AOD (lidar, nonspherical)/AOD (lidar, spherical + nonspherical) ratios. The latter represents a dust fraction index. Red and blue squares denote results from in situ measurements assuming all coarse particles are dust and NaCl (+ water), respectively. The AAODs derived from in situ measurements are systematically higher and lower for low-dust and high-dust cases, respectively.

are several possible reasons for the underestimates in the in situ values. First, because b_{ext} is lower for coarse particles (in situ measurements) compared with nonspherical particles (lidar measurements), the contribution from dust light absorption could be underestimated. When the aerosol absorption coefficient (b_{abs}) is scaled with a same scaling factor to be used for b_{ext} (coarse particles) to agree with the lidar values (nonspherical particles), the AAOD underestimate of in situ measurements decreases from 36–40% to 6–19%. Second, although the refractive index of $1.51 \pm 0.0041i$ at 500 nm reported by *Aoki et al.* [2005] is used in this study, this value has uncertainty. Finally, dust particles coated with BC may increase the light absorption efficiency [e.g., *Kim et al.*, 2005]. These results suggest that the current estimate of light absorption by dust particles has uncertainties although it is essential to separate the dust contribution from BC light absorption.

4. Uncertainties in the AAOD Estimate From In Situ Data

4.1. Optical Calculation Method and Mixing State

[33] In this section, uncertainties in the AAOD estimates from in situ BC data are examined (Table 4). First, a ±15% uncertainty was estimated for the BC mass concentrations from SP2 measurements [*Moteki and Kondo*, 2010] (section 2.1). Second, the contribution from the altitudes below the aircraft measurement was estimated to be 20% of the AAOD for the 5 April case (section 2.2). An uncertainty in this contribution was estimated to be ±20% of the total AAOD (100% error for the low-level contribution). This second uncertainty is shown as the error bars in Figure 5.

[34] To estimate uncertainties resulting from various assumptions used for aerosol optical calculations from in situ aerosol measurements, sensitivity calculations were performed for AAOD (Figure 8). Results for 5 April are shown here as an example (high AOD and low dust), and similar results were obtained for the other cases. Figure 8 shows the relative change in the AAODs relative to the base case calculation; the resulting AAODs in the sensitivity calculations were divided by 0.0222, i.e., the AAOD of base case calculation with the NaCl assumption. For reference, the AAODs derived from the sky radiometer measurements (2 h average and standard deviation) divided by 0.0222 are shown with blue horizontal lines.

[35] Figure 8 (left) shows results calculated with different BC mixing state assumptions and optical calculation methods. A k value (imaginary part of the refractive index) of 0.79 (used for the base case calculation) was used for these sensitivity calculations. The first sensitivity calculation was performed assuming that a particle was homogeneous with an effective refractive index estimated using the Maxwell-Garnett mixing rule. This mixing rule can be used for many insoluble particles (BC) suspended in solution ($(NH_4)_2SO_4$ + water). For the refractive index of a solution, the volume average mixing rule was used. The core-shell model (adopted in this study) and the Maxwell-Garnett model are two commonly used methods in advanced aerosol model calculations [e.g., *Lesins et al.*, 2002; *Stier et al.*, 2007]. *Adachi et al.* [2010] showed that absorption cross sections estimated using the Maxwell-Garnet effective medium method agreed better (within 10%) with those obtained with the detailed optical calculations (discrete dipole approximation (DDA)) as compared with other methods (including the core-shell model) using 46 standard particles with different BC shapes and positions within the host particles. When the Maxwell-Garnett model was used in this study, the AAOD agrees with the core-shell model result within 9% (the Maxwell-Garnett model result is larger). It is noted that the BC shape (morphology), which is also an important factor for calculating the AAOD, was not examined in this study. Further investigations are necessary for the aerosol optical calculation method to correctly account for the particle morphology.

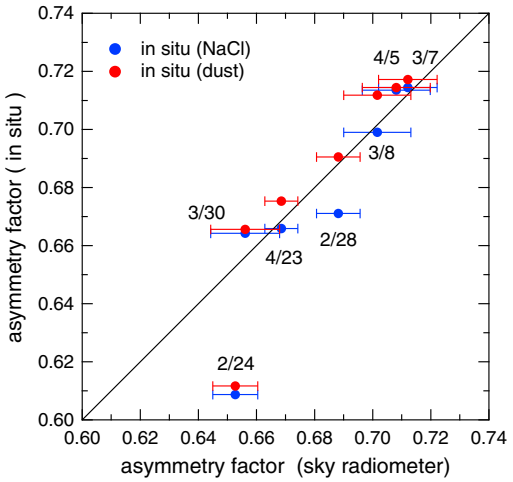

Figure 7. Comparison of the asymmetry factor g between aircraft (in situ) and sky radiometer measurements. Red and blue circles denote results from in situ measurements assuming all coarse particles are dust and NaCl (+ water), respectively. The uncertainties (error bars) are the same as in Figure 4.

Table 4. Uncertainties in AAOD Calculations From In Situ Data (Upper Limit)

Source	Uncertainty
BC mass concentration	±15%
Contribution from the altitudes below the aircraft measurement	±20%
Refractive index of BC	±8%
BC mixing state	+9% and −18%
Contribution from organic aerosol (OA) and dust	+36%
Overall (root-sum-square)	+45% and −32%

[36] The second AAOD was calculated assuming all BC particles are bare spherical particles (no coating). Coating materials enhanced BC absorption by a factor of 1.57 for the case we examined here (using the core-shell model). This level of enhancement (lensing effect) is similar to that found for air experiencing a half day of transport after leaving BC source regions [*Oshima et al*., 2009]. We note here that the AAOD for bare BC particles agrees with sun-sky photometer measurements better (within 24%) than that calculated with the lensing effect (within 50% for the base calculation). A smaller lensing effect is possible when the BC is off-centered position or attached to the surface of its host material [*Adachi et al*., 2010; *Sedlacek et al*., 2012]. In fact, a very small lensing effect (approximately 6% at 532 nm) was reported from observations in an urban center [*Cappa et al*., 2012]. However, during the A-FORCE-2013W experiment, filter sampling on board the aircraft followed by electron tomography [*Adachi et al*., 2010] indicated that most BC particles were coated (surrounded) with other aerosol compounds instead of being attached to BC-free particles or present without any coating (K. Adachi, personal communication, 2013). Consequently, the AAODs calculated without lensing effect (bare BC particle assumption) were quite likely underestimated. The uncertainty in AAOD estimates that arises from the BC mixing state uncertainty is estimated to be +9% (Maxwell-Garnett model) and −18% (half the difference with the bare BC particle assumption). A more extensive discussion on the lensing effect is beyond the scope of this study. More ground-based experiments are required to resolve this issue.

[37] For the third sensitivity calculation, the AAOD for dry conditions was calculated. Although humidity increases the AOD value by 39% on average (NaCl case), the AAOD changes by only 3.1%. The increase in the BC coating thickness due to aerosol-phase water results in only small changes in light absorption because the lens effect is saturated [*Bond et al*., 2006]. Therefore, although humidity increases the SSA, the AAOD exhibits only small changes.

[38] For the fourth and fifth sensitivity calculations, simpler mixing state assumptions, which have been widely used in regional and global models, were adopted, although these assumptions are known to be unrealistic. For the fourth calculation, a single mixing state assumption was adopted for fine particles ($D_{dry} < 850$ nm in this study, as described in section 2). With this assumption, all particles in the fine mode have the same mixing state. The total (bulk) volume concentrations of BC and other compounds ($(NH_4)_2SO_4$ + water) were calculated by summing both BC-containing and BC-free particles. The BC and other compounds were then redistributed using the aerosol (shell) size distribution assuming that the volume fraction of BC and other compounds is the same within all particles. Optical calculations were made using the core-shell model. With this assumption, the AAOD increased by a factor of 2.0. For the fifth calculation, a homogeneous mixing state assumption is used by prescribing the volume average refractive index between BC and other compounds (gray particle assumption). As a result, the AAOD increases slightly (15%) from the value obtained

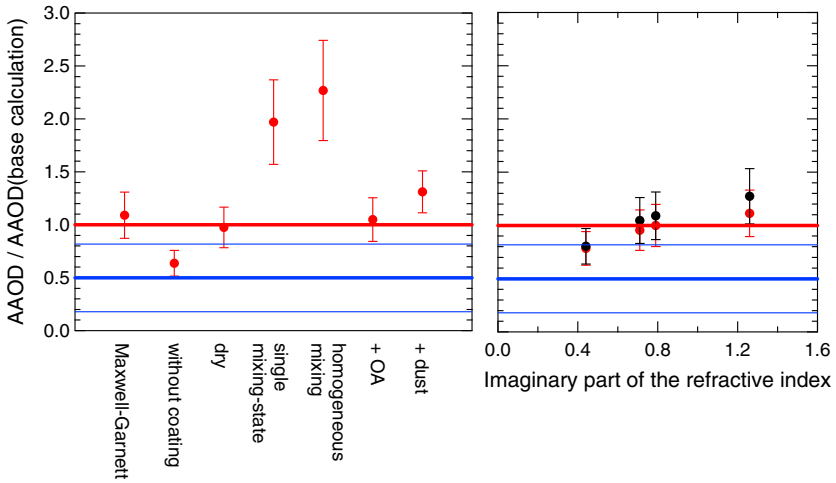

Figure 8. AAODs calculated with various different assumptions. A relative change in the AAOD compared to the base case calculation with the NaCl assumption is shown. Values observed on 5 April were used for the aerosol size distribution and BC mixing state. The three blue lines indicate the sky radiometer measurements (average and standard deviation). (left) Maxwell-Garnett mixing rule for the refractive index, bare BC particles (no coating), dry conditions (no aerosol-phase water), single mixing state with the simple volume mixing rule, and homogeneous mixing state (gray particle), including light absorption of organic aerosol (HULIS) and of dust particles. See text for additional details. (right) Dependence of the AAOD on the imaginary part of the BC refractive index (k) listed in Table 2. Red and black circles denote the results obtained with the core-shell and the Maxwell-Garnett models, respectively.

with the single mixing state assumption. The large increase in the AAOD for the single mixing state or gray particle assumption is because all particles absorb radiation and the total surface area of absorbing particles increases. In other words, a separation between BC-containing and BC-free particles is essential for aerosol optical calculation, which has been indicated by previous studies, e.g., *Oshima et al*. [2009] and *Matsui et al*. [2013].

[39] For the last sensitivity calculation, absorption from organic aerosol (OA) was included. The contribution from dust particles (31%) is also shown for reference, although this value is likely overestimated considering that the coarse particle AOD (in situ) is greater than the nonspherical particle AOD (lidar) by a factor of 1.5 for the 5 April case. In the base case calculations, all BC coating material and BC-free fine particles were assumed to consist of $(NH_4)_2SO_4$ + water. When OA was included, 50% of the bulk non-BC compound volume (BC coating material + BC-free fine particles) was assumed to consist of OA. Moreover, 6% of the bulk OA volume was assumed to consist of humic-like substance (HULIS). These assumptions are based on aerosol measurements at the Gosan site, which is located near the Fukue Observatory [*Miyazaki et al*., 2007]. For the imaginary part of the refractive indices (k) of HULIS, 0.039 was used [*Dinar et al*., 2008; *Kirchstetter et al*., 2004] (Table 2). As a result, the AAOD increases by only 5%. It has been reported that the light absorption of these aerosol compounds increases in the near-ultraviolet region and the contribution at visible wavelengths is not as large. The uncertainty from OA and dust at 500 nm was estimated to be +36%.

4.2. Refractive Index of BC

[40] Figure 8 (right) shows the AAOD dependence on the imaginary part of the BC refractive index (k). As described in section 2.2, a k value of 0.79 was used for the base calculations as recommended by *Bond and Bergstrom* [2006]. For the sensitivity calculations, we used k values of 0.71 (middle level of values provided by *Bond and Bergstrom* [2006] at 550 nm), 0.44 (Optical Properties of Aerosols and Clouds (OPAC) database [*Hess et al*., 1998]), and 1.26 (at 1064 nm) [*Moteki et al*., 2010b] (Table 2). The value reported for 1064 nm was used because the wavelength dependence of the refractive index is likely negligible. The results from two different optical calculation methods are shown. The first method is the core-shell optical calculation method, which was used throughout this study (red circles). Figure 8 shows that the AAOD changes by only 35% for a factor of 3 change in the k. When the OPAC value is excluded, following the recommendation of *Bond and Bergstrom* [2006], the AAOD change decreases to 16% (±8%). Although this value is not small when atmospheric heating effects are considered, the uncertainty is smaller than several other uncertainties described above (Table 4).

[41] The other results (black circles) shown in Figure 8 (right) were calculated using the Maxwell-Garnett method. Similar to the findings for the core-shell model, the dependence of the Maxwell-Garnett AAOD on k is relatively weak; when the OPAC value is excluded (i.e., difference between $k = 0.71$ and 1.26), the AAOD difference is 20% (±10%). In summary, the two best optical calculation methods currently available predict similar AAOD dependence on k for the cases examined in this study. As long as these methods are used, a choice of the refractive index introduces only a relatively small error.

[42] It is noted, however, that when the particle diameter is relatively small (much smaller than 60 nm when $1.95 + 0.79i$ is assumed for the BC refractive index at 500 nm), the Rayleigh-Gans approximation is valid and the particle absorption cross section increases linearly with the imaginary part of the refractive index [*Bohren and Huffman*, 1998]. Although both the core-shell and Maxwell-Garnett models predict a more moderate dependence of the AAOD on k, the dependence can be potentially larger.

[43] The overall uncertainty (upper limit) was estimated by taking a root-sum-square of the individual uncertainties described above to be +45% and −32% (Table 4).

5. Conclusions

[44] We report the first attempt to compare the aerosol absorption properties calculated from in situ SP2 measurements of BC and ground-based sun-sky photometer measurements (sky radiometer measurements from SKYNET). Comparisons are performed for the seven cases in which the research aircraft made vertical profile measurements near the Fukue Observatory in the East China Sea during the A-FORCE-2009 (spring) and -2013W (late winter) experiments. The aerosol extinction coefficients (b_{ext}) and SSA were calculated based on total aerosol size distributions and detailed BC mixing state information for fine particles assuming that all coarse particles are dust or NaCl (+ water). In these calculations, BC and dust are the only two light absorbers and an enhancement in BC light absorption by the lens effect is estimated using detailed observed BC mixing state information and adopting the core-shell optical calculation method. The seven cases were classified into groups according to AOD (AOD > 0.4 or not) and dust fraction (nonspherical contribution to the total AOD smaller than 0.2 or greater than 0.4). The AOD criterion arises because SSA retrieval is reliable only when the AOD is greater than 0.4 according to the data selection criteria of both AERONET [*Dubovik et al*., 2000] and SKYNET [*Hashimoto et al*., 2012].

[45] Good agreements are found for both the calculated extinction coefficients and AODs from in situ data with lidar and sky radiometer measurements, respectively. The AOD estimates from the in situ measurements agreed with the sky radiometer measurements within 12 ± 18% and 2 ± 8% for high-AOD and low-dust cases, respectively. Generally, the fine- and coarse-particle b_{ext} values derived from the in situ measurements agree with the lidar-derived spherical and nonspherical particle estimates, respectively, suggesting that most coarse particles were dust on these days.

[46] Only one case (5 April) satisfies both the high-AOD and low-dust criteria. In this case, the sky radiometer-derived AAOD at 500 nm is approximately a factor of 2 smaller than those calculated from in situ data even when all coarse particles were assumed to be NaCl, which does not absorb radiation at 500 nm. The other two low-dust cases (30 March and 23 April) exhibit similar results, although the AODs were lower than 0.4 (0.16 and 0.19, respectively). Because the mass absorption cross section (MAC = AAOD/column-BC-mass) estimated from the sky radiometer-derived AAOD and in situ BC mass measurements is also systematically lower by a factor of 2 compared with previous measurements, this result suggests a

potential negative bias in the AAODs from sky radiometer measurements. An accurate surface albedo estimate was found to be critical for sky radiometer retrieval analyses. Because the AAOD measurements made by sun-sky radiometers are currently the only constraint available for estimates of global BC radiative forcing, more investigation is required to validate these measurements.

[47] On the other hand, under high-dust conditions, the sky radiometer measurements provide systematically higher AAODs for the two high-AOD cases (7 and 8 March). The AAODs derived from in situ measurements could be underestimated because of a possible underestimate in dust contributions, uncertainty in the dust refractive index, and BC coating of dust particle surface. To accurately estimate the atmospheric heating effect caused by BC, it is essential to separate the contribution of dust to aerosol light absorption.

[48] **Acknowledgments.** We are indebted to all A-FORCE participants for their cooperation and support. Special thanks are due to the flight and ground crews of the DAS King Air aircraft for helping make this effort a success. We thank Ikuyo Oshima for her contributions to the data analyses. We also thank Kouji Adachi at the Meteorological Research Institute, Japan, for providing electron tomography information of BC and useful comments. We also thank Yugo Kanaya at the Japan Agency for Marine-Earth Science and Technology (JAMSTEC) for providing COSMOS BC data and Teruyuki Nakajima at the Atmosphere and Ocean Research Institute, University of Tokyo, for his useful comments and suggestions. This study was supported by the Ministry of Education, Culture, Sports, Science, and Technology (MEXT) in Japan (Grant-in-Aid for Scientific Research (S) and GRENE Arctic Climate Change Research Project), the strategic international cooperative program of the Japan Science and Technology Agency (JST), and the global environment research fund of the Japanese Ministry of the Environment (2A-1101).

References

Adachi, K., S. H. Chung, and P. R. Buseck (2010), Shapes of soot aerosol particles and implications for their effects on climate, *J. Geophys. Res.*, *115*, D15206, doi: 10.1029/2009JD012868.

Aoki, T., T. Y. Tanaka, A. Uchiyama, M. Chiba, M. Mikami, S. Yabuki, and J. R. Key (2005), Sensitivity experiments of direct radiative forcing caused by mineral dust simulated with a chemical transport model, *J. Meteorol. Soc. Jpn.*, *83A*, 315–331.

Arnott, W. P., K. Hamasha, H. Moosmuller, P. J. Sheridan, and J. A. Ogren (2005), Towards aerosol light-absorption measurements with a 7-wavelength aethalometer: Evaluation with a photoacoustic instrument and 3-wavelength nephelometer, *Aerosol Sci. Technol.*, *39*, 68–83.

Arnott, W. P., J. W. Walker, H. Moosmuler, R. A. Elleman, H. H. Jonsson, G. Buzorius, W. C. Conant, R. C. Flagan, and J. H. Seinfeld (2006), Photoacoustic insight for aerosol light absorption aloft from meteorological aircraft and comparison with particle soot absorption photometer measurements: DOE Southern Great Plains climate research facility and the coastal stratocumulus imposed perturbation experiments, *J. Geophys. Res.*, *111*, D05S02, doi:10.1029/2005JD005964.

Bohren, C. F., and D. R. Huffman (1998), *Absorption and Scattering of Light by Small Particles*, John Wiley, Hoboken, N. J.

Bond, T. C., and R. W. Bergstrom (2006), Light absorption by carbonaceous particles: An investigative review, *Aerosol Sci. Technol.*, *40*, 27–67.

Bond, T., T. L. Anderson, and D. Campbell (1999), Calibration and intercomparison of filter-based measurements of visible light absorption by aerosols, *Aerosol Sci. Technol.*, *30*, 582–600.

Bond, T. C., G. Habib, and R. W. Bergstrom (2006), Limitations in the enhancement of visible light absorption due to mixing state, *J. Geophys. Res.*, *111*, D20211, doi:10.1029/2006JD007315.

Bond, T., et al. (2013), Bounding the role of black carbon in the climate system: A scientific assessment 2013, *J. Geophys. Res. Atmos.*, *118*, 5380–5552, doi:10.1002/jgrd.50171.

Cappa, C. D., et al. (2012), Radiative absorption enhancements due to the mixing state of atmospheric black carbon, *Science*, *337*, 1078–1081.

Che, H., G. Shi, A. Uchiyama, A. Yamazaki, H. Chen, P. Goloub, and X. Zhang (2008), Intercomparison between aerosol optical properties by a PREDE skyradiometer and CIMEL sunphotometer over Beijing, China, *Atmos. Chem. Phys.*, *8*, 3199–3214, doi:10.5194/acp-8-3199-2008.

Cheng, Y. F., et al. (2009), Influence of soot mixing state on aerosol light absorption and single scattering albedo during air mass aging at a polluted regional site in northeastern China, *J. Geophys. Res.*, *114*, D00G10, doi:10.1029/2008JD010883.

Chung, C. E., V. Ramanathan, and D. Decremer (2012), Observationally constrained estimates of carbonaceous aerosol radiative forcing, *Proc. Natl. Acad. Sci. U. S. A.*, *109*, 11,624–11,629.

Corrigan, C. E., G. C. Roberts, M. V. Ramana, D. Kim, and V. Ramanathan (2008), Capturing vertical profiles of aerosols and black carbon over the Indian Ocean using autonomous unmanned aerial vehicles, *Atmos. Chem. Phys.*, *8*, 737–747.

Dinar, E., A. Abo Riziq, C. Spindler, C. Erlick, G. Kissc, and Y. Rudich (2008), The complex refractive index of atmospheric and model humic-like substances (HULIS) retrieved by a cavity ring down aerosol spectrometer (CRD-AS), *Faraday Discuss.*, *137*, 279–295.

Dubovik, O., A. Smirnov, B. Holben, M. D. King, Y. J. Kaufman, T. F. Eck, and I. Slutsker (2000), Accuracy assessment of aerosol optical properties retrieval from Aerosol Robotic Network (AERONET) sun and sky radiance measurements, *J. Geophys. Res.*, *105*, 9791–9806.

Dubovik, O., B. Holben, T. F. Eck, A. Smirnov, Y. J. Kaufman, M. D. King, D. Tanr´e, and I. Slutsker (2002), Variability of absorption and optical properties of key aerosol types observed in worldwide locations, *J. Atmos. Sci.*, *59*, 590–608.

Esteve, A. R., J. A. Ogren, P. J. Sheridan, E. Andrews, B. N. Holben, and M. P. Utrillas (2012), Sources of discrepancy between aerosol optical depth obtained from AERONET and in-situ aircraft profiles, *Atmos. Chem. Phys.*, *12*, 2987–3003.

Hale, G. M., and M. R. Querry (1973), Optical constants of water in the 200-nm to 200-Mm wavelength region, *Appl. Optics*, *12*, 555–563.

Hashimoto, M., T. Nakajima, O. Dubovik, M. Campanelli, H. Che, P. Khatri, T. Takamura, and G. Pandithurai (2012), Development of a new data-processing method for SKYNET sky radiometer observations, *Atmos. Meas. Tech.*, *5*, 2723–2737.

Hess, M., P. Koepke, and I. Schult (1998), Optical properties of aerosols and clouds: The software package OPAC, *Bull. Am. Meteorol. Soc.*, *79*(5), 831–844.

Kanakidou, M., et al. (2005), Organic aerosol and global climate modelling: A review, *Atmos. Chem. Phys.*, *5*, 1053–1123.

Kanaya, Y., F. Taketani, Y. Komazaki, X. Liu, Y. Kondo, L. K. Sahu, H. Irie, and H. Takashima (2013), Comparison of black carbon mass concentrations observed by multi-angle absorption photometer (MAAP) and continuous soot-monitoring system (COSMOS) on Fukue Island and in Tokyo, Japan, *Aerosol Sci. Technol.*, *47*(1), 1–10, doi:10.1080/02786826.2012.716551.

Katagiri, S., et al. (2010), Cirrus cloud radiative forcing derived from synergetic use of MODIS analyses and ground-based observations, *SOLA*, *6*, 025–028, doi:10.2151/sola.2010-007.

Kim, D.-H., J. Sohn, T. Nakajima, and T. Takamura (2005), Aerosol radiative forcing over east Asia determined from ground-based solar radiation measurements, *J. Geophys. Res.*, *110*, D10S22, doi:10.1029/2004JD004678.

Kirchstetter, T. W., T. Novakov, and P. V. Hobbs (2004), Evidence that the spectral dependence of light absorption by aerosols is affected by organic carbon, *J. Geophys. Res.*, *109*, D21208, doi:10.1029/2004JD004999.

Koike, M., N. Takegawa, N. Moteki, Y. Kondo, H. Nakamura, K. Kita, H. Matsui, N. Oshima, M. Kajino, and T. Y. Nakajima (2012), Measurements of regional-scale aerosol impacts on cloud microphysics over the East China Sea: Possible influences of warm sea surface temperature over the Kuroshio ocean current, *J. Geophys. Res.*, *117*, D17205, doi:10.1029/2011JD017324.

Kondo, Y. L., et al. (2009), Stabilization of the mass absorption cross section of black carbon for filter-based absorption photometry by the use of a heated inlet, *Aerosol Sci. Technol.*, *43*, 741–756.

Kondo, Y., L. Sahu, N. Moteki, F. Khan, N. Takegawa, X. Liu, M. Koike, and T. Miyakawa (2011), Consistency and traceability of black carbon measurements made by laser-induced incandescence, thermal-optical transmittance, and filter-based photo-absorption techniques, *Aerosol Sci. Technol.*, *45*, 295–312, doi:10.1080/02786826.2010.533215.

Lesins, G., P. Ch´ylek, and U. Lohmann (2002), A study of internal and external mixing scenarios and its effect on aerosol optical properties and direct radiative forcing, *J. Geophys. Res.*, *107*(D10), 4094, doi:10.1029/2001JD000973.

Matsui, H., M. Koike, Y. Kondo, N. Moteki, J. D. Fast, and R. A. Zaveri (2013), Development and validation of a black carbon mixing state resolved three-dimensional model: Aging processes and radiative impact, *J. Geophys. Res. Atmos.*, *118*, 2304–2326, doi:10.1029/2012JD018446.

Miyazaki, Y., Y. Kondo, S. Han, M. Koike, D. Kodama, Y. Komazaki, H. Tanimoto, and H. Matsueda (2007), Chemical characteristics of water-soluble organic carbon in the Asian outflow, *J. Geophys. Res.*, *112*, D22S30, doi:10.1029/2007JD009116.

Moteki, N., and Y. Kondo (2007), Effects of mixing state on black carbon measurements by laser-induced incandescence, *Aerosol Sci. Technol.*, *41*, 398–417.

Moteki, N., and Y. Kondo (2010), Dependence of laser-induced incandescence on physical properties of black carbon aerosols: Measurements and theoretical interpretation, *Aerosol Sci. Technol.*, *44*(8), 663–675, doi:10.1080/02786826.2010.484450.

Moteki, N., Y. Kondo, T. Nakayama, K. Kita, L. Sahu, T. Ishigai, T. Kinase, and Y. Matsumi (2010a), Radiative transfer modeling of filter-based measurements of light absorption by particles: Importance of particle size dependent penetration depth, *J. Aerosol Sci.*, *41*, 401–412.

Moteki, N., Y. Kondo, and S. Nakamura (2010b), Method to measure refractive indices of small nonspherical particles: Application to black carbon particles, *J. Aerosol Sci.*, *41*, 513–521.

Moteki, N., Y. Kondo, N. Oshima, N. Takegawa, M. Koike, K. Kita, H. Matsui, and M. Kajino (2012), Size dependence of wet removal of black carbon aerosols during transport from the boundary layer to the free troposphere, *Geophys. Res. Lett.*, *39*, L13802, doi:10.1029/2012GL052034.

Nakajima, T., G. Tonna, R. Rao, Y. Kaufman, and B. Holben (1996), Use of sky brightness measurements from ground for remote sensing of particulate polydispersions, *Appl. Optics*, *35*, 2672–2686.

Nakajima, T., et al. (2007), Overview of the Atmospheric Brown Cloud East Asian Regional Experiment 2005 and a study of the aerosol direct radiative forcing in East Asia, *J. Geophys. Res.*, *112*, D24S91, doi:10.1029/2007JD009009.

Oshima, N., M. Koike, Y. Zhang, and Y. Kondo (2009), Aging of black carbon in outflow from anthropogenic sources using a mixing state resolved model: 2. Aerosol optical properties and cloud condensation nuclei activities, *J. Geophys. Res.*, *114*, D18202, doi:10.1029/2008JD011681.

Oshima, N., et al. (2012), Wet removal of black carbon in Asian outflow: Aerosol Radiative Forcing in East Asia (A-FORCE) aircraft campaign, *J. Geophys. Res.*, *117*, D03204, doi:10.1029/2011JD016552.

Petters, M. D., and S. M. Kreidenweis (2007), A single parameter representation of hygroscopic growth and cloud condensation nucleus activity, *Atmos. Chem. Phys.*, *7*, 1961–1971.

Redemann, J., S. J. Masonis, B. Schmid, T. L. Anderson, P. B. Russell, J. M. Livingston, O. Dubovik, and A. D. Clarke (2003), Clear-column closure studies of aerosols and water vapor aboard the NCAR C-130 during ACE-Asia, 2001, *J. Geophys. Res.*, *108*(D23), 8655, doi:10.1029/2003JD003442.

Ricchiazzi, P., C. Gautier, J. A. Ogren, and B. Schmid (2006), A comparison of aerosol optical properties obtained from in situ measurements and retrieved from sun and sky radiance observations during the May 2003 ARM Aerosol Intensive Observation Period, *J. Geophys. Res.*, *111*, D05S06, doi:10.1029/2005JD005863.

Sedlacek, A., and J. Lee (2007), Photothermal interferometric aerosol absorption spectrometry, *Aerosol Sci. Technol.*, *41*, 1089–1101.

Sedlacek, A. J., E. R. Lewis, L. Kleinman, J. Xu, and Q. Zhang (2012), Determination of and evidence for non-core-shell structure of particles containing black carbon using the single-particle soot photometer (SP2), *Geophys. Res. Lett.*, *39*, L06802, doi:10.1029/2012GL050905.

Shimizu, A., N. Sugimoto, I. Matsui, K. Arao, I. Uno, T. Murayama, N. Kagawa, K. Aoki, A. Uchiyama, and A. Yamazaki (2004), Continuous observations of Asian dust and other aerosols by polarization lidars in China and Japan during ACE-Asia, *J. Geophys. Res.*, *109*, D19S17, doi:10.1029/2002JD003253.

Shinozuka, Y., A. D. Clarke, S. G. Howell, V. N. Kapustin, C. S. McNaughton, J. Zhou, and B. E. Anderson (2007), Aircraft profiles of aerosol microphysics and optical properties over North America: Aerosol optical depth and its association with PM2.5 and water uptake, *J. Geophys. Res.*, *112*, D12S20, doi:10.1029/2006JD007918.

Sokolik, I. N., and O. B. Toon (1999), Incorporation of mineralogical composition into models of the radiative properties of mineral aerosol from UV to IR wavelengths, *J. Geophys. Res.*, *104*, 9423–9444.

Stier, P., J. H. Seinfeld, S. Kinne, and O. Boucher (2007), Aerosol absorption and radiative forcing, *Atmos. Chem. Phys.*, *7*, 5237–5261.

Streets, D. G., et al. (2003), An inventory of gaseous and primary aerosol emissions in Asia in the year 2000, *J. Geophys. Res.*, *108*(D21), 8809, doi:10.1029/2002JD003093.

Takegawa, N., and H. Sakurai (2011), Laboratory evaluation of a TSI condensation particle counter (model 3771) under airborne measurement conditions, *Aerosol Sci. Technol.*, *45*(2), 272–283.

Takegawa, N., N. Moteki, M. Koike, N. Oshima, and Y. Kondo (2013), Condensation particle counters combined with a low-pressure impactor for fast measurement of mode-segregated aerosol number concentration, *Aerosol Sci. Technol.*, *47*, 1059–1065.

Tomikawa, Y., and K. Sato (2005), Design of the NIPR trajectory model, *Polar Meteorol. Glaciol.*, *19*, 120–137.

Toon, O. B., J. B. Pollack, and B. N. Khare (1976), The optical constants of several atmospheric aerosol species: Ammonium sulfate, aluminum oxide, and sodium chloride, *J. Geophys. Res.*, *81*, 5733–5748.

Zaveri, R. A., J. C. Barnard, R. C. Easter, N. Riemer, and M. West (2010), Particle-resolved simulation of aerosol size, composition, mixing state, and the associated optical and cloud condensation nuclei activation properties in an evolving urban plume, *J. Geophys. Res.*, *115*, D17210, doi:10.1029/2009JD013616.